PROCEEDINGS, Thirty-Sixth Workshop on Geothermal Reservoir Engineering
Stanford University, Stanford, California, January 31 - February 2, 2011
SGP-TR-191

MICRO-SEISMICITY, FAULT STRUCTURE AND HYDRAULIC COMPARTMENTALIZATION WITHIN THE COSO GETHERMAL FIELD, CALIFORNIA

J. Ole Kaven[a,b], Stephen H. Hickman[a], and Nicholas C. Davatzes[b]

[a]U.S.Geological Survey,
345 Middlefield Road, MS 977
Menlo Park, CA 94025

[b]EES Temple University,
1901 N. 13th St,
Philadelphia, PA, 19122, USA
e-mail: okaven@usgs.gov

ABSTRACT

High precision earthquake locations and subsurface velocity structure provide potential insights into fracture system geometry, fluid conduits and fluid compartmentalization critical to geothermal reservoir management. We analyze 16 years of seismicity to improve hypocentral locations and simultaneously invert for the seismic velocity structure within the Coso Geothermal Field (CGF). The CGF has been continuously operated since the 1980's and is separated into two main compartments: the main field and the east flank. These compartments are at higher temperatures than the immediate surroundings. We find that relocated seismicity in the main field is shallower than in the east flank and occurs at the same depths as the injection and production wells, while the east flank seismicity extends about 1 km below the injection and production wells and is occurring almost exclusively in regions of high temperature. In the east flank, many of the earthquakes appear to align along planar features, suggesting through-going, pre-existing faults that may act as conduits for fluid and heat transport. The seismic velocity structure is heterogeneous, with compressional wave speed (Vp) generally lower in the main field when compared to the east flank and shear wave speed (Vs) varying more significantly in the shallow portions of the reservoir. The Vp/Vs ratio appears to outline the two main compartments of the reservoir, with a narrow zone of relatively high Vp/Vs separating the main field from the east flank. In the deeper portion of the reservoir this zone becomes less prominent. Several factors influence Vp/Vs ratios in geothermal systems including temperature, fracture geometry/density, and fluid saturation or pore pressure. Comparison of the distribution of Vp/Vs ratios with a temperature model generated from well logs reveals a first-order correlation between regions of low Vp/Vs ratio and high temperature. However, there is a better correlation between the distribution of production-induced microseismicity and Vp/Vs ratio, especially where high seismicity density occurs within the regions of high temperature, suggesting that these low Vp/Vs ratios most likely result from changes in fluid saturation or pore pressure.

INTRODUCTION

The Coso Geothermal Field (CGF), located east of the Sierra Nevada batholith, is situated in a tectonically active region that features strike-slip and normal faults as well as numerous magmatic intrusions evident at the surface as rhyolite domes (Duffield et al., 1980; Davatzes and Hickman, 2006). At least two groups of faults can be distinguished at the surface based on their orientation and style of faulting (Fig. 1): west-north-west trending faults with dextral strike-slip that form prominent lineaments with uncertain ages (Duffield et al., 1980) and north to north-east trending normal faults that dip both west and east that may have been active in the Quaternary (Hulen, 1978; Davatzes and Hickman, 2006). These faults appear to roughly divide the reservoir into two distinct compartments: the main field and the east flank (Fig.1). These compartments, which encompass smaller hydrologic compartments within them, also feature the highest temperatures in the CGF (Fig.2).

Seismicity within the CGF occurs both naturally (tectonic events) and as a consequence of injection and production within the field. Seismicity is recorded by the Navy Geothermal Program Office (GPO) and initial locations by the GPO generally reveal diffuse clouds of seismicity that occur predominantly in the main field and the east flank. These clouds are not clearly coincident with mapped fault traces at the surface, and thus the fault structure at depth remains poorly constrained.

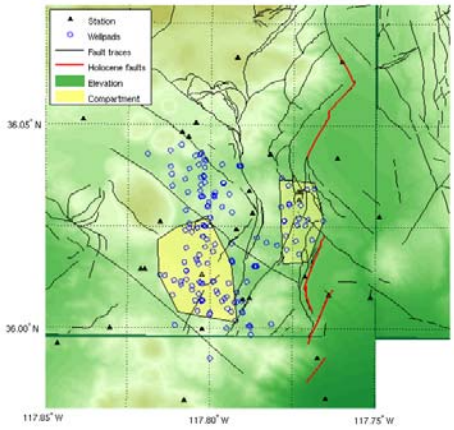

Figure 1: Map of the Coso Geothermal Field (CGF). Yellow shaded polygons indicate the approximate extent of the two main compartments of the CGF (main field and east flank) and were defined using subsurface temperature contours from Fig. 2 and wellhead locations (shown here as circles). Note that the east flank polygon disregards regions of indicated high temperature to the north (Fig. 2) due to insufficient spatial coverage of well temperature data in that area of the field. The locations of seismic stations used in this study are shown as triangles, along with Quaternary fault traces (red where Holocene or younger; see Davatzes and Hickman, 2006, for details.)

Numerous studies have used data recorded by the GPO and surrounding SCSN/USGS networks. Some of these studies analyzed earthquakes within and adjacent to the CGF to improve hypocentral locations and invert for the velocity structure of the greater Coso area (e.g. Lees, 1998; Wu and Lees, 1999; Hauksson and Unruh, 2007), while others have focused on improving hypocentral locations and obtaining moment tensors for microseismicity associated with individual hydraulic fracturing events (Foulger et al. 2008; Julian et al., 2010). In a regional study of subsurface variations in compressional (Vp) and shear (Vs) velocities from July 1993 to June 1995, Wu and Lees (1999) found low Vp/Vs ratios in the main field at geothermal production depths, which they suggest might represent a hot, fluid-depleted zone. Time-varying seismic tomography by Julian et al. (2008) from 1996 through 2006 indicate a decrease in Vp/Vs with time in the upper 2km of the CGF main field, which they suggest may indicate mineral dehydration or a decrease in fluid saturation due to reservoir depletion.

The goal of our investigation is to better constrain the subsurface geometry of faults that may act as either conduits or barriers to fluid migration and to define the nature and extent of hydrologic compartmentalization within the CGF. To accomplish this, we improve field-wide hypocentral locations of earthquakes that were recorded on the Navy GPO network and invert for the velocity structure of the CGF at finer resolution than Julian et al. (2008). Our analyses are similar in resolution and spatial coverage to those of Wu and Lees (1999), but we utilize 12 years of additional data. Also, unlike Wu and Lees (1999), we perform simultaneous velocity inversions and earthquake relocations using double-difference techniques to better constrain both the subsurface velocity structure and the distribution of microseismicity.

DATA & METHODS

We use catalog P- and S-wave arrival times determined by the Navy GPO from April 1996 to October 2008. Data is recorded at 20 permanent and 30 temporarily deployed stations, most of which are three-component seismometers sampling at either 480Hz or 250Hz. The GPO catalog contains >60,000 earthquakes in the greater Coso region during the time period studied. We decimate the catalog by including only earthquakes in the region outlined in Fig. 3 with recorded magnitudes $\geq$0.5 to permit field-wide velocity inversions. This leaves 10,200 earthquakes, 2.4 million P-wave arrival times and 1.13 million S-wave arrival times, which were used to relocate and invert for the seismic velocity structure. We are currently carrying out waveform cross-correlations for the recorded events to improve the resolution of our inversions, but differential travel times from cross-correlated events are not included in this study.

Relocating seismicity using double-difference techniques is based on the premise that two earthquakes in close proximity to one another recorded at the same stations travel through the same subsurface structure (Waldhauser and Ellsworth, 2000). The structure along the travel paths of the seismic rays is one of the main contributors to errors in location (Schaff et al., 2002). Thus, by using differential travel times of two earthquakes that travel along essentially the same paths, these ray path effects can be eliminated and errors in relative location are typically reduced by one to two orders of magnitude (Schaff et al. 2004). The drawback of this method is that locations are only known relative to one another, but absolute arrival times can be used to "reference" the relocated catalog (Zhang and Thurber, 2003).

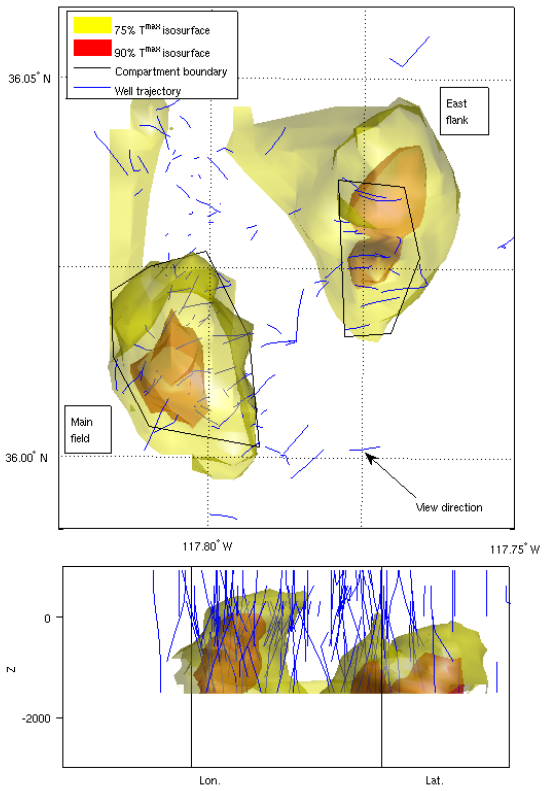

Figure 2: Well trajectories (blue lines) within the CGF and transparent temperature isosurfaces, normalized to the maximum temperature recorded downhole, Tmax; where yellow is 75% of Tmax; and red is 90% of Tmax. Temperature isosurfaces were interpolated from well temperature logs. Top panel: map view; bottom panel: cross-sectional view looking south-east to north-west (see top panel for view direction). Temperature isosurfaces were truncated at 1500 m below mean sea level due to insufficient well log data below that depth.

In actively producing geothermal reservoirs the velocity structure is often highly heterogeneous in three dimensions (Wu and Lees, 1999), which necessitates the use of earthquake location algorithms that allow for the simultaneous solution of three-dimensional velocity structure. We employ the double-difference earthquake relocation and velocity inversion code *tomoDD* that uses a pseudo-bending ray tracing algorithm to find the seismic rays and calculate travel times between events and stations (Zhang and Thurber, 2003). The resulting velocity model is represented as nodes in three dimensions and the velocity values are calculated and linearly interpolated between adjacent nodes. We start with the horizontally homogeneous 1-D velocity model with constant Vp/Vs ratio of 1.73 of Julian and Foulger (2010) and iteratively update the seismic velocity structure. We display resultant body wave speeds only if sufficient ray path coverage exists between nodes to ensure robust results (DWS>10; see Evans et al., 1994). Nodes have horizontal and vertical spacing of 0.5km. We display the final step at which seismic velocities at the nodes and event locations are not subject to significant changes from the pen-ultimate iteration.

To compare the results of earthquake relocations and velocity inversions from *tomoDD* to regions of high temperature and high productivity in the field, we utilize well log temperature data compiled from 1985 to 2003 provided by the Navy GPO. These data were linearly interpolated between wells to produce continuous, three-dimensional distributions of temperatures throughout the CGF (Fig.2). We display relative instead of absolute temperature to avoid showing data that might be proprietary. In Fig. 2 and subsequent figures, we plot well trajectories to show the extent of the reservoir at the surface and at depth.

RESULTS AND DISUCUSSION

Relocations

Although seismicity following double-difference relocation is still diffuse (Fig.4), comparison to catalog earthquake locations (Fig. 3) shows that earthquakes tend to condense into tighter, more distinct clusters following relocation, in both plan view and in cross section. In addition, relocation demonstrates even more clearly that seismicity in the east flank is generally deeper than in the main field, and continues downward about a kilometer below the deepest reach of the wells (Fig. 4 bottom). Hauksson and Unruh (2007) suggest that the brittle-ductile transition bulges upward underneath the main field, perhaps in response to elevated temperatures, leaving the deeper portions of the main field void of seismicity. Relocation also reveals two prominent seismic lineaments in cross section, both in the main field and in the east flank. Although the main field lineament was also visible in the catalog locations (Fig. 3 bottom), the east flank lineament is significantly accentuated following relocation (Fig. 4 bottom, shown by arrow). These lineaments are most evident when viewed in the north-northeast direction (see view direction depicted in Fig. 4, top), which is approximately parallel to the dominant structural trend of faults mapped at the surface (Fig. 1). Thus, although there is no clear one-to-one correspondence between these lineaments and specific faults mapped at the surface, these seismic lineaments may represent fault zones extending to depth that act as preferential conduits for heat and fluid transport from overlying geothermal wells. If so, the changes in

fluid pressure and thermal regime associated with fluid migration along these fault zones might explain why these zones are more seismically active than the adjacent host rock.

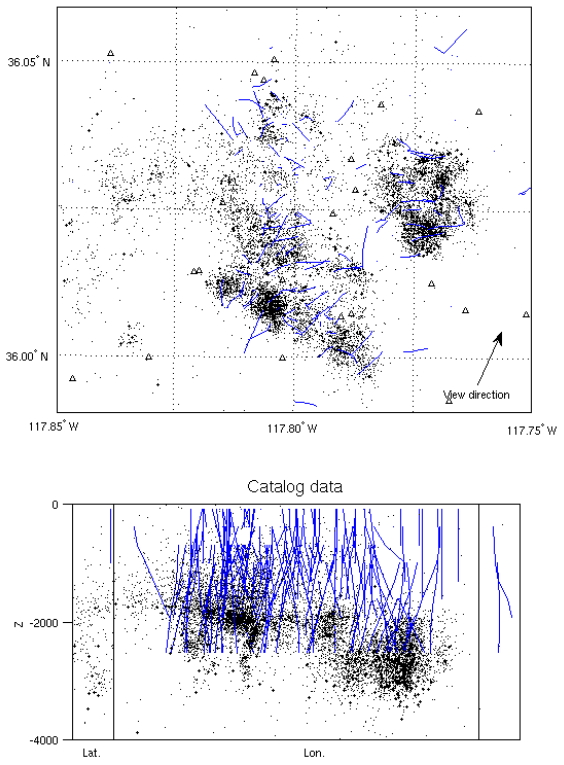

Figure 3: Catalog seismicity (black dots, filled circles for M>2) in map view (top panel) and horizontal view (bottom panel). Well trajectories are shown as blue lines. Arrow in top panel shows view direction for depth section in bottom panel. Depths are in meters, and are computed assuming that all seismic stations are at an elevation of mean sea level (z=0); i.e., without taking actual station elevations into account. Well depths have been adjusted to the z=0 elevation.

Comparison of relocated seismicity with interpolated temperature isosurfaces (Fig. 5) reveals that earthquakes in the east flank are clearly associated with regions of elevated temperature, with very little seismicity outside the high-temperature region. Although east flank seismicity is generally below the interpolated isotherms, we contend that downward continuation of these isosurfaces is reasonable and indicates elevated temperatures at even greater depth. Although seismicity in the main field is more diffuse, it also shows a tendency to be associated with regions of higher-than-average subsurface temperature (Fig. 5). Since most of the microseismicity in the CGF is production-induced, this correlation between elevated temperatures and seismicity suggests that the main field and the east flank constitute distinct, relatively permeable hydrologic compartments that are sites of natural hydrothermal upwelling and inter-well pressure communication.

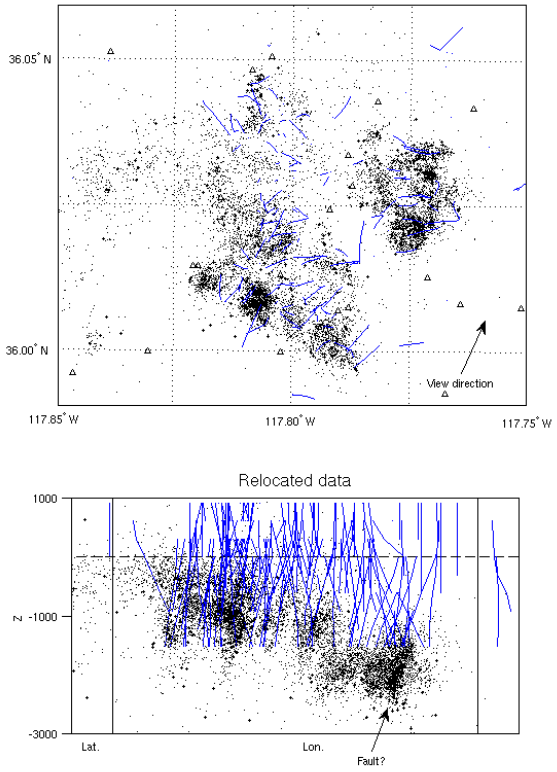

Figure 4: Relocated seismicity (black dots, filled circles for M>2) in map view (top panel) and horizontal view (bottom panel). Well trajectories are shown as blue lines. Arrow in top panel shows view direction for depth section in bottom panel. Depth, z, is in meters relative to mean sea level (dashed line in bottom panel), with relocated seismicity and well trajectories truncated at the minimum station elevation (996m). Unlike the catalog locations, these relocations take into account the actual elevations of the GPO seismic stations.

We anticipate that improved double-difference earthquake relocations using cross-correlated waveforms within the CGF will elucidate a more detailed fault structure than is evident from catalog travel-time relocations alone. Nevertheless, the continuation of seismic lineaments to considerable depth below the east flank wells suggests that fluid flow along preexisting, through-going faults may

play an important role in establishing pressure and thermal communication between geothermal production and injection wells and the deeper portions of the field.

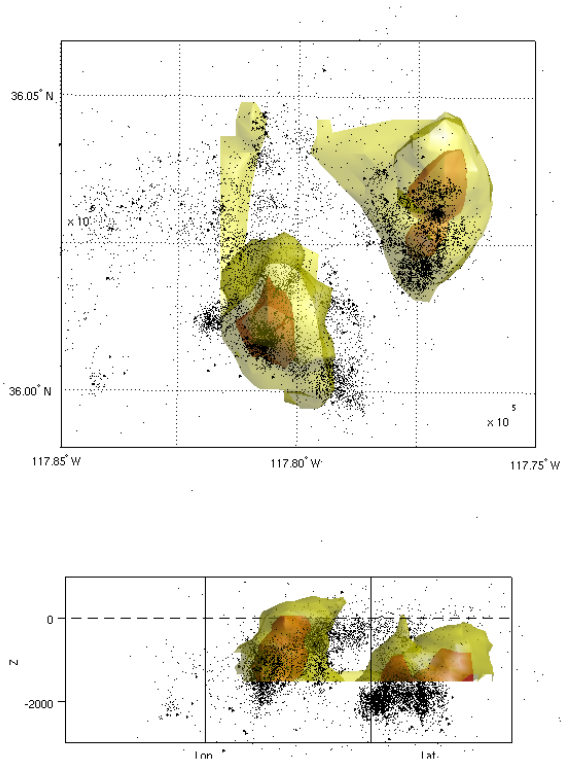

Figure 5: Temperature isosurfaces and relocated seismicity (black dots, filled circles for M>2) in map view (top panel) and cross-section view (bottom panel) looking from south-east to north-west; see arrow in top panel of Fig.2 for view direction. Color scale for isosurfaces is the same as in Fig. 2.

Seismic velocity structure

The seismic velocity structure obtained from our inversion reveals heterogeneous distributions of Vp and Vs along horizontal slices through the field (Fig.6). In the shallow portion of the CGF (z = 0 km, with all depths discussed herein relative to mean sea level), Vp is higher in both the main field and east flank when compared to adjacent portions of the field. At greater depths (z = 1.5 to 3 km), high Vp is evident only in the east flank. In contrast, Vs varies more smoothly than Vp, with Vs exhibiting relative highs near the east flank and the main field at shallow to intermediate depths (z = 0 to 1.5 km). However, in the deeper portion of the field (z = 2 km) the highest Vs is found midway between the east flank and the main field.

Julian et al. (2008) suggest that regions of high Vs within the main field may reflect decreases in fluid pressure relative to adjacent portions of the field. This is consistent with our observation of relatively high Vs within both the east flank and the main field at depths of 0 to 1.5 km, approximately coincident with seismicity associated with ongoing geothermal production (Fig. 4, bottom). It is also interesting to note that the presence of relatively high Vp at depths of 1.5 to 3 km beneath the east flank but not the main field mirrors the greater depth extent of seismicity beneath the east flank (Fig 4). However, this lobe of high Vp extends below the deepest earthquakes in the east flank, thus the relationship (if any) between this relatively high Vp and geothermal production is not clear.

The ratio of shear to compressional wave speeds (Vp/Vs ratio) is commonly used to infer sub-surface variations in rock and fluid properties, with Vp/Vs being most sensitive to changes in temperature, effective stress (normal stress minus pore pressure), porosity/pore geometry (including fractures), and fluid saturation state (e.g., Wu and Lees, 1999). The initial 1-D velocity model with which we start this inversion (Julian and Foulger, 2010) has a constant Vp/Vs ratio of 1.73. Following our 3-D inversion, this ratio ranges from 1.54 to 1.92 throughout the CGF (Fig. 6), with a mean value for all grid points of 1.72.

Regions of low Vp/Vs can be found at all depths within the CGF (Fig. 6). However, clear lobes of low Vp/Vs are associated with both the main field and the east flank at a depth of 1 km and to a lesser extent at 1.5 km, which are separated by a northwest-southeast trending “ridge” of high Vp/Vs. At greater depths this separation diminishes, and low Vp/Vs ratios are prevalent both within and between the east flank and main field.

In low porosity crystalline rock, such as the granitic rocks comprising the CGF, decreases in Vp/Vs ratio are generally attributed to increases in temperature or decreases in porosity, water saturation and/or fluid pressure (O'Connell and Budiansky, 1974; Chatterjee et al., 1985). Since seismicity associated with geothermal production is present in both portions of the CGF at depths of 1 to 1.5 km (Fig. 4), we postulate that these localized decreases in Vp/Vs are most likely due to relatively low water saturation or fluid pressure due to ongoing geothermal production or may result from naturally elevated temperatures within the main field and east flank (Fig. 2).

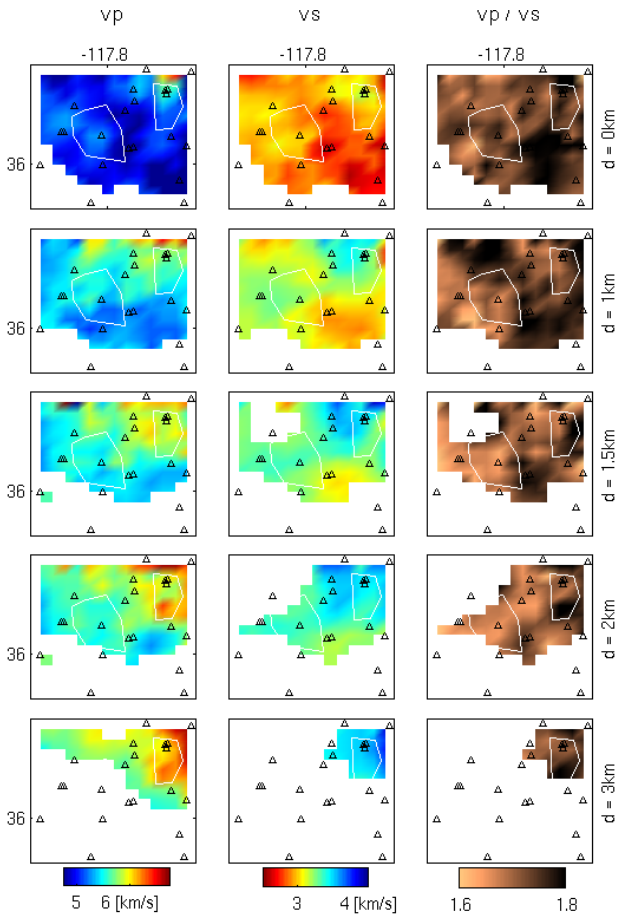

Figure 6: Inverted seismic velocities: Vp (left column), Vs (middle column), and Vp/Vs (right column) with increasing depth relative to mean sea level. White polygons highlight the approximate extents of the main field and east flank compartment (Fig. 1). Black triangles show GPO seismic station. Results are only displayed when sufficient ray path crossing occur near the inversion nodes (see text).

In order to examine more closely possible correlations between temperature and Vp/Vs ratio within the CGF, we compare the depth distribution of Vp/Vs against subsurface temperature at depths for which both parameters are well constrained (Fig. 7). This comparison reveals that at shallow depths (≤ 0 km) Vp/Vs ratios are poorly correlated with temperature, while at depths of 0.5 km and (especially) 1 km the regions of highest temperature are well correlated with low Vp/Vs, and clearly outline the east flank and main field.

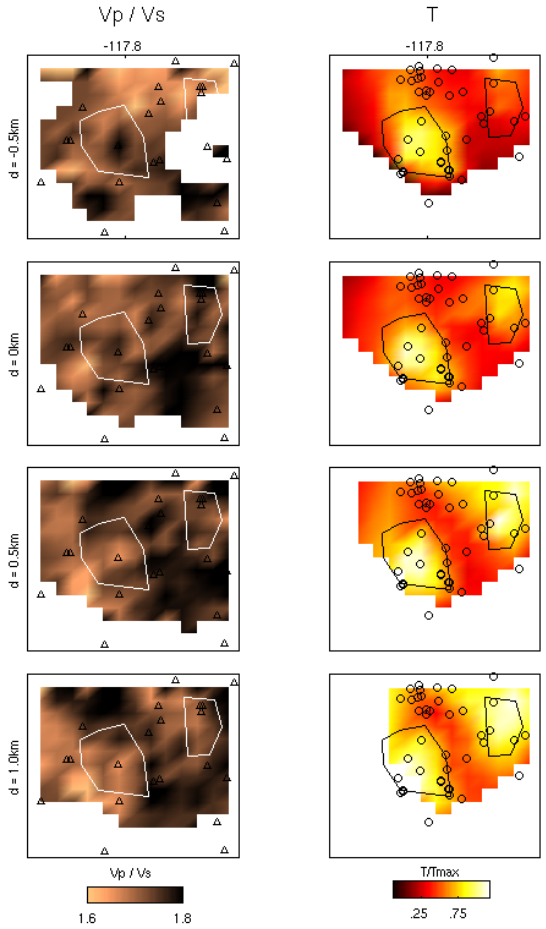

Figure 7: Inverted Vp/Vs (left column) with increasing depths compared to temperature (right column) from well log data, represented as horizontal slices through the isosurfaces depicted in Fig. 2.

It is important to note that microseismicity associated with geothermal production is prevalent in both the main field and east flank at a depth of 1 km (Fig. 4), where the spatial correlation between low Vp/Vs and the two main compartments of the CGF is the strongest (Fig. 7). At depths shallower than this, the Vp/Vs anomaly defining the main field and east flank diminishes (at a depth of 0.5 km) and then disappears altogether (at depths of 0 and -0.5 km), in spite of high subsurface temperatures. Thus, we suggest that variations in Vp/Vs observed within the CGF are most likely the result of decreases in water saturation or fluid pressure within the main field and east flank and not the result of high elevated temperatures

Note that the "ridge" of high Vp/Vs separating the main field from the east flank at depths of 0.5 and 1 km is spatially correlated with a northwest-southeast extending zone of low temperatures (Fig. 7). This correlation together with the observation that this intervening region is almost devoid of seismicity (Fig. 4), suggests the absence of major conduits for fluid and heat transport between the two hydrothermal compartments comprising the CGF. We anticipate that the inclusion of waveform cross-correlated differential travel times currently underway will permit greater resolution of subsurface velocity variations and relative earthquake relocations within the CGF. This will lead to improved constraints on the nature and extent of hydrothermal compartmentalization and the role of faults as conduits to fluid and heat transport within the CGF.

CONCLUSIONS

Double-difference techniques and catalog P- and S-wave arrival times are used to simultaneously relocate earthquakes with magnitudes greater than 0.5 from 1996 to 2008 and determine subsurface velocity structure in the Coso Geothermal Field (CGF). This analysis reveals that diffuse clouds of seismicity visible from catalog locations tend to sharpen into more distinct volumes and structural features following relocation. These structural features may, in part, control fluid and heat flow in the two main producing compartments of the CGF: the main field and the east flank. Seismicity in the main field extends along the depths of injection and production wells with generally diffuse clouds of seismicity. In contrast, seismicity in the east flank extends deeper than the wells, in some cases along linear features, and is confined to regions exhibiting higher temperatures than adjacent portions of the CGF. The seismicity clusters within planar zones below the wells in the east flank, suggesting that large-scale, through-going faults may be involved in the transport of fluids and heat in this portion of the reservoir. The general strike of one of these faults is in agreement with the trend of faults mapped at the surface, although there is not a clear one-to-one correlation between specific surface faults and seismicity.

Simultaneous inversion for the three-dimensional P- and S-wave velocity structure within the CGF updates the analyses of Wu and Lees (1999) with 12 years of additional data. High S-wave velocity (Vs) and to a lesser extent high P-wave velocity (Vp) are associated with both the east flank and main field at depths comparable to ongoing geothermal production. Furthermore, the Vp/Vs ratio is relatively low within the main field and east flank at depths of 1.0 to 1.5 km below sea level (~2.0 to 2.5 km below land surface), with these two regions of low Vp/Vs being separated by a continuous zone of high Vp/Vs. This separation, when combined with the lack of observable seismicity between the main field and east flank, further suggests that these two portions of the field act as distinct hydrologic compartments.

Subsurface temperature isosurfaces constructed from well log data reveal high-temperature regions beneath the main field and east flank that are approximately co-located with the regions exhibiting low Vp/Vs ratios in the CGF. However, these regions of low Vp/Vs correlate better with microseismicity induced by geothermal production within these high-temperature volumes than they do with subsurface temperature. Thus, although the causes for the low Vp/Vs ratios seen beneath the main field and east flank cannot be known with certainty, we suggest that this may be a result of decreases in fluid saturation and/or fluid pressure within the active geothermal reservoir.

ACKNOWLEDGEMENTS

We thank the Navy GPO and Terra-Gen for permission to use their seismic and temperature data. We also thank Bruce Julian, Steve Bjornstad, Wei-Chuang Huang, and Jess McCulloch for helpful discussions regarding Coso seismic data, hydrogeology and neotectonics and Colin Williams and Justin Rubinstein for critical reviews of this paper. This work was funded by the *DOE Geothermal Technologies Program* under Interagency Agreement DE-EE0001501, with additional support provided by the USGS Energy Resources and Earthquake Hazards Programs.

REFERENCES

Chatterjee, S.N., Pitt, A.M., and Iyer, H.M. (1985), "Vp/Vs ratios in the Yellowstone National Park Region, Wyoming" *Journal of Volcanology and Geothermal Research*, **26**, 213-230.

Davatzes, N. C. and Hickman, S. H.. (2006), "Stress and faulting in the Coso geothermal field: update and recent results from the East Flank and Coso Wash" *Proceedings 31st Workshop on geothermal Reservoir Engineering, Stanford University, Stanford, California, January 30 – February 1. 2006,* SGP-TR-179, 12p.

Duffield, W. A., Bacon, C. R., and Dalrymple, G. B. (1980), "Late Cenozoic volcanism, geochronology and structure of the Coso Range, Inyo County, California" *Journal of Geophysical Research*, **85**, 2381-2404.

Evans, J.R., Eberhart-Phillips, D. and Thurber, C.H. (1994), "User's manual for SIMULPS12 for imaging Vp and Vp/Vs: a derivative of the "Thurber" tomographic inversion SIMUL3 for local earthquakes and explosions" *U.S.Geological Survey, Open File Report*, 94-431, 100pp.

Foulger, G.R., Julian, B.R. And Monastero, F. C. (2008), "Seismic monitoring of EGS tests at the Coso Geothermal area, California, using accurate MEQ locations and full moment tensors" *Proceedings 33rd Workshop on geothermal Reservoir Engineering, Stanford University, Stanford, California, January 28 – 30, 2008,* SGP-TR-179, 8p.

Hauksson, E. and Unruh, J. (2007), "Regional tectonics of the Coso geothermal area along the intracontinental plate boundary in central eastern California: Three-dimensional Vp and Vp/Vs models, spatio-temporal seismicity patterns, and seismogenic deformation" *Journal of Geophysical Research*, **112**, B06309.

Hulen, J. B. (1978), "Geology and alteration of the Coso geothermal area, Inyo County, California" *U.S. Dept. of Energy: Geothermal Energy*.

Julian, B.R., Foulger, G.R. And Monastero, F. C. (2008), "Time-dependent seismic tomography and its application to the Coso Geothermal Area, 1996-2006" *Proceedings 33rd Workshop on geothermal Reservoir Engineering, Stanford University, Stanford, California, January 28 – 30, 2008,* SGP-TR-185, 4p.

Julian, B.R., G.R. Foulger, F.C. Monastero and S. Bjornstad (2010), "Imaging Hydraulic Fractures in a Geothermal Reservoir", *Geophys. Res. Lett., 37*, L07305, 10.1029/2009GL040933

Lees, J. M. (1998), "Multiplet Analyses at Coso Geothermal" *Bulletin of the Seism. Soc. America*, **88**, no.5, 1127-1143.

O'Connell, R.J., and Budiansky, B. (1974), "Seismic velocities in dry and saturated cracked solids" *Journal of Geophysical Research*, **79**, no. 35 5412-5426.

Schaff, D.P., Bokelmann, G.H.R., Beroza, G.C., Waldhauser, F., and Ellsworth, W.L. (2002) "High resolution image of the Calaveras Fault seismicity" *Journal of Geophysical Research*, **107**, no.B9, 2186, doi 10.1029/2001JB000633.

Schaff, D.P., Bokelmann, G.H.R., Ellsworth, W.L., Zanzerkia, E., Waldhauser, F., and Beroza, G.C. (2004), "Optimizing correlation techniques for improved earthquake location" *Bulletin of the Seism. Soc. America*, **94**, no.2, 705-7021.

Waldhauser, F. and Ellsworth, W.L. (2000), "A double-difference earthquake location algorithm: method and application to the northern Hayward Fault, California", *Bulletin of the Seism. Soc. America*, **90**, 1353-1368.

Wu, E. and Lees, J. M. (1999), "Three-dimensional P and S wave velocity structures of the Coso Geothermal Area, California, from microseismic travel time" *Journal of Geophysical Research*, **104**, no. B6, 13217-13233.

Zhang, H. and Thurber, C.H. (2003), "Double-Difference tomography: the method and its application to the Hayward Fault, California", *Bulletin of the Seism. Soc. America*, **93**, no.5 1875-1889.